

The optical variability of flat-spectrum radio quasars in the SDSS Stripe 82 region

Minfeng Gu^{1,2} and Y. L. Ai^{3,4}

¹ Key Laboratory for Research in Galaxies and Cosmology, Shanghai Astronomical Observatory, Chinese Academy of Sciences, 80 Nandan Road, Shanghai 200030, China
e-mail: gumf@shao.ac.cn

² Department of Physics, University of California, Santa Barbara, CA 93106, USA

³ National Astronomical Observatories/Yunnan Observatory, Chinese Academy of Sciences, P.O. Box 110, 650011 Kunming, Yunnan, China

⁴ Key Laboratory for the Structure and Evolution of Celestial Objects, Chinese Academy of Sciences, P.O. Box 110, 650011 Kunming, Yunnan, China

Preprint online version: May 31, 2018

ABSTRACT

Context. Although a bluer-when-brighter trend is commonly observed in blazars, the opposite trend of redder-when-brighter has also been found in some blazars.

Aims. We investigate the frequency of the redder-when-brighter trend in flat-spectrum radio quasars (FSRQs).

Methods. We investigate the optical variability of 29 FSRQs in the SDSS Stripe 82 region using SDSS DR7 released multi-epoch data covering about nine years. We determined the spectral index by fitting a powerlaw to SDSS *ugriz* photometric data, and explored the relationship between the spectral index and source brightness.

Results. For all FSRQs studied, we detect variations in *r* band flux of overall amplitude between 0.24 mag and 3.46 mag in different sources. Fourteen of 29 FSRQs display a bluer-when-brighter trend. However, only one source exhibits a redder-when-brighter trend, which implies that this behavior is rare in our FSRQ sample. In this source, the thermal emission from the accretion disk may be responsible for the redder-when-brighter trend.

Key words. galaxies: active – galaxies: quasars: general – galaxies: photometry

1. Introduction

Blazars, including BL Lac objects and flat-spectrum radio quasars (FSRQs), are the most extreme class of active galactic nuclei (AGNs), characterized by strong and rapid variability, high polarization, and apparent superluminal motion. These extreme properties are generally interpreted as a consequence of non-thermal emission from a relativistic jet oriented close to the line of sight. As such, they represent a fortuitous natural laboratory with which to study the physical properties of jets, and, ultimately, the mechanisms of energy extraction from central supermassive black holes.

While the jet nonthermal emission is generally thought to be the most dominant type in FSRQs, this is not always true. Chen, Gu & Cao (2009a) found that thermal emission can be the most significant at least in optical bands for some FSRQs selected from the SDSS DR3 quasar catalogue. The emission of FSRQs is indeed a mixture of thermal emission from accretion disk and jet nonthermal emission. As thermal emission generally does not vary much as clearly evident in radio-quiet AGNs (e.g. Ai et al. 2010), any variations in the emission of FSRQs could be dominated by variations in the jet nonthermal component. Consequently, the ratio of thermal to nonthermal emission varies at different source flux states. This may cause variations in the spectral shape where, for example, the color becomes redder when the source is brighter as shown in Gu et al. (2006). In principle, the details of spectral variability may largely depend

on the ratio of thermal to nonthermal emission, and the characteristics of variations in each component.

The color/spectral behavior can be used to explore the emission mechanisms in blazars, which remain unclear. The bluer-when-brighter trend (BWB) is commonly observed in blazars, especially BL Lac objects (e.g. Ghisellini et al. 1997; Fan et al. 1998; Massaro et al. 1998; Ghosh et al. 2000; Clements & Carini 2001; Raiteri et al. 2001; Villata et al. 2002; Vagnetti et al. 2003; Wu et al. 2005, 2007; Rani et al. 2010), which can usually be explained with shock-in-jet models. However, the opposite trend, i.e. redder-when-brighter trend (RWB) has also been found (e.g. Ghosh et al. 2000; Gu et al. 2006; Rani et al. 2010). The several examples are 3C 446 (Miller 1981), PKS 0735+178 (Ghosh et al. 2000), PKS 0736+017 (Clements et al. 2003; Ramírez et al. 2004), PKS 0420-014 and 3C 454.3 (Gu et al. 2006), and PKS 1622-297 and CTA 102 (Osterman Meyer et al. 2008, 2009). The situation even may be more complicated because no clear color trend has been reported in some cases (e.g. Ghosh et al. 2000; Stalin et al. 2006; Böttcher et al. 2007; Poon et al. 2009). Although there have been many studies of the color behavior of FSRQs, not many FSRQs have been found to display a redder-when-brighter trend. Moreover, while BL Lac objects display in general a bluer-when-brighter trend, it is unclear whether a redder-when-brighter trend is generally present in FSRQs (Gu et al. 2006; Hu et al. 2006; Rani et al. 2010). In this work, we investigate the spectral variability of FSRQs, to help us establish how common the redder-when-brighter trend is in FSRQs.

The layout of this paper is as follows: in Section 2, we describe the source sample; the variability results are outlined in Section 3; Section 4 includes the discussion; and in the last section, we draw our conclusions. The cosmological parameters $H_0 = 70 \text{ km s}^{-1} \text{ Mpc}^{-1}$, $\Omega_m = 0.3$, and $\Omega_\Lambda = 0.7$ are used throughout the paper, and the spectral index is defined as $f_\nu \propto \nu^{-\alpha}$, where f_ν is the flux density at frequency ν .

2. Sample selection

2.1. Quasars in Stripe 82 region

Our initial quasar sample was selected as those quasars both in the SDSS DR7 quasar catalogue (Schneider et al. 2010) and Stripe 82 region. The SDSS DR7 quasar catalogue consists of 105,783 spectroscopically confirmed quasars with luminosities brighter than $M_i = -22.0$, with at least one emission line having a full width at half-maximum (FWHM) larger than 1000 km s^{-1} and highly reliable redshifts. The sky coverage of the sample is about 9380 deg^2 and the redshifts range from 0.065 to 5.46. The five-band (u, g, r, i, z) magnitudes have typical errors of about 0.03 mag. The spectra cover the wavelength range from 3800 to 9200 \AA with a resolution of ≈ 2000 (see Schneider et al. 2010 for details). The Stripe 82 region, i.e. right ascension $\alpha = 20^{\text{h}} - 4^{\text{h}}$ and declination $\delta = -1^{\circ}.25 - +1^{\circ}.25$, was repeatedly scanned during the SDSS-I phase (2000 - 2005) under generally photometric conditions, and the data are well calibrated (Lupton et al. 2002). This region was also scanned repeatedly over the course of three 3-month campaigns in three successive years in 2005 - 2007 known as the SDSS Supernova Survey (SN survey). The multi-epoch photometric observations therefore enable us to investigate the optical variability of the selected quasars.

2.2. Cross-correlation with radio catalogues

In this paper, we define a quasar to be a FSRQ according to its radio spectral index. Therefore, we cross-correlate the initial quasar sample with the Faint Images of the Radio Sky at Twenty centimeters (FIRST) 1.4-GHz radio catalogue (Becker, White & Helfand 1995), the Green Bank 6-cm (GB6) survey at 4.85 GHz radio catalogue (Gregory et al. 1996), and the Parkes-MIT-NRAO (PMN) radio continuum survey at 4.85 GHz (Griffith & Wright, 1993), as well as for sources with $\delta < 0^\circ$. The FIRST survey used the Very Large Array (VLA) to observe the sky at 20 cm (1.4 GHz) with a beam size of 5.4 arcsec. FIRST was designed to cover the same region of the sky as the SDSS, and observed 9000 deg^2 at the north Galactic cap and a smaller $2^\circ.5$ wide strip along the celestial equator. It is 95 per cent complete to 2 mJy and 80 per cent complete to the survey limit of 1 mJy. The survey contains over 800,000 unique sources, with an astrometric uncertainty of $\lesssim 1$ arcsec.

The GB6 survey at 4.85 GHz was executed with the 91-m Green Bank telescope in 1986 November and 1987 October. Data from both epochs were assembled into a survey covering the $0^\circ < \delta < 75^\circ$ sky down to a limiting flux of 18 mJy, with 3.5 arcmin resolution. GB6 contains over 75,000 sources, and has a positional uncertainty of about 10 arcsec at the bright end and about 50 arcsec for faint sources (Kimball & Ivezić 2008). The PMN surveys were made using the Parkes 64-m radio telescope at a frequency of 4850 MHz with the NRAO multibeam receiver mounted at the prime focus (Griffith & Wright 1993). The surveys had a spatial resolution of approximately $4'.2$ FWHM and were made for the southern sky between declinations of -87° and $+10^\circ$, and all right ascensions during June and November

in 1990. The positional accuracy is close to 10 arcsec in each coordinate. The survey was divided into four declination bands. One of these four is the equatorial survey ($-9^\circ.5 < \delta < +10^\circ.0$) covering 1.90 sr, which contains 11,774 sources to a flux limit of 40 mJy and largely overlaps the GB6 survey in the declination range from 0° to $+10^\circ$ (Griffith et al. 1995).

The initial quasar sample was first cross-correlated between the SDSS quasar positions and the FIRST catalogue to within 2 arcsec (see e.g. Ivezić et al. 2002; Lu et al. 2007). The resulting sample of SDSS quasar positions was then cross-correlated with both the GB6 and PMN equatorial catalogues to within 1 arcmin (e.g. Kimball & Ivezić 2008). Owing to the different spatial resolutions of FIRST, GB6, and PMN, multiple FIRST counterparts were found to within 1 arcmin for some quasars, although there is only single GB6 and/or PMN counterparts existed. The flux density of the closest FIRST counterparts may be dominant among multiple counterparts in some sources, although not in others. In this paper, we conservatively selected the sources with single FIRST counterparts to within 1 arcmin of the SDSS positions. This selection criterion, for example, helps avoid the contamination of genuine steep-spectrum radio quasars (SSRQs). These SSRQs may appear as multi-FIRST components, but be identified as FSRQs if using the flux density of the closest FIRST component, which is actually much smaller than that of radio lobes. The optical variability of quasars with multiple FIRST counterparts will be presented in a forthcoming paper.

A sample of 37 quasars was constructed from the above cross-correlations. The radio spectral index α was then calculated between the FIRST 1.4 and either or both of the GB6 and PMN 4.85 GHz. Finally, 32 quasars were conventionally defined as FSRQs, with $\alpha < 0.5$, and the remaining five quasars are SSRQs with $\alpha > 0.5$. When counterparts were found in both the GB6 and PMN surveys, the spectral indices were consistent with each other.

2.3. Sample

Our final sample of 32 FSRQs is listed in Table 1, which provides the source redshift, radio loudness, radio spectral index, black hole mass, disc bolometric luminosity, and the Eddington ratio, and the similar data of five SSRQs are listed for comparison. The distribution of redshift, radio loudness, black hole mass, and the Eddington ratio are shown in Fig. 1. The source redshift is taken directly from the SDSS DR7 quasar catalogue, which covers $0.4 < z < 2.7$. The radio loudness is from Shen et al. (2010), which ranges from $\log R = 1.97$ (SDSS J005205.56+003538.1) to $\log R = 4.48$ (SDSS J222646.53+005211.3). However, the radio loudness was calculated as $R = f_{6\text{cm}}/f_{2500}$, where $f_{6\text{cm}}$ and f_{2500} are the flux density at rest-frame 6 cm and 2500 \AA , respectively (see Shen et al. 2010 for more details). Among 32 FSRQs, 14 sources have an inverted spectral index between 1.4 and 4.85 GHz with $\alpha < 0$.

Black hole masses are estimated from the various empirical relations in the literature by using the luminosity and FWHM of broad H β , Mg II, and C IV lines, i.e., Vestergaard & Peterson (2006) for H β , and Kong et al. (2006) for Mg II and C IV. The luminosity and FWHM of broad H β , Mg II, and C IV lines are adopted from the measurements in Shen et al. (2010). The BLR luminosity L_{BLR} is derived following Celotti, Padovani & Ghisellini (1997) by scaling the strong broad emission lines H β , Mg II, and C IV to the quasar template spectrum of Francis et al. (1991), in which Ly α is used as a flux reference of 100. By adding the contribution of H α with a value of 77, the total rela-

tive BLR flux is 555.77, which consists of H β at 22, Mg II at 34 and C IV at 63 (Francis et al. 1991; Celotti et al. 1997). From the BLR luminosity, we estimate the disc bolometric luminosity as $L_{\text{Bol}} = 10L_{\text{BLR}}$ (Netzer 1990). The black hole mass ranges from $10^{7.7}M_{\odot}$ to $10^{9.4}M_{\odot}$, most of sources being in $10^{8.5} - 10^{9.0}M_{\odot}$ range, which is typical of blazars (Ghisellini et al. 2010). The Eddington ratio $\log L_{\text{Bol}}/L_{\text{Edd}}$ ranges from -1.96 to 0.57, with most sources being in the -1.0 - 0.0 range, which is indicative of a standard thin disk (Shakura & Sunyaev 1973) being present in all FSRQs.

3. Results

The SDSS DR7 CAS contains the Stripe82 database, containing all imaging from SDSS stripe 82 along the celestial equator at the southern Galactic cap. It includes a total of 303 runs, covering any given piece of the close to 270 deg² area approximately 80 times. Only about one-quarter of the stripe 82 scans were obtained in photometric conditions, the remainder being taken under variable clouds and often poorer than normal seeing. For the runs that were non-photometric, an approximate calibration, using the photometric frames as reference, was derived and made available in the CAS Stripe82 database. In this work, we directly use the point-spread-function magnitudes in the CAS Stripe82 database from the photometric data obtained during the SDSS-I phase from data release 7 (DR7; Abazajian et al. 2009) and the SN survey during 2005 - 2007. The typical measurement error in magnitude is about 0.03 mag.

Among 32 FSRQs, we select the sources classified as point sources in all observational runs. Only data with good measurements (high-quality photometry) are selected following the recommendations in the SDSS instructions¹. Moreover, we insist on the *ugriz* magnitude being brighter than the magnitude limit in each band, i.e. 22.0, 22.2, 22.2, 21.3, 20.5 at *u, g, r, i, z*, respectively. The data taken at cloudy conditions are also excluded. We calculate the spectral index from the linear fit to the $\log f_{\nu} - \log \nu$ relation after applying an extinction correction to the *ugriz* flux density and taking the flux error into account. In most cases, the linear fit gave good fits. Each cycle of *ugriz* photometry was usually completed within five minutes, i.e. quasi-simultaneously, therefore, the spectral index calculation will not be seriously influenced by any source variations.

3.1. Variability

Among 32 FSRQs, three sources were excluded from our analysis for various reasons. SDSS J015243.14+002039.6 is classified as a galaxy in the SDSS pipeline, although it is classified as a quasar in the SDSS DR7 quasar catalogue. The images of SDSS J215349.75+003119.5 are usually saturated because of a nearby bright object. Owing to the low quality of the *u* band images, SDSS J222646.53+005211.3 was also excluded because we aim to derive the spectral index using only high quality *ugriz* photometric data.

All remaining 29 FSRQs show large amplitude variations with overall variations in *r* band $\Delta r = 0.24 - 3.46$ mag (see Table 1), which is much larger than that of radio quiet AGNs, 0.05 - 0.3 mag (e.g. Ai et al. 2010), but typical of blazars (e.g. Gu et al. 2006). There are four sources with $\Delta r > 1$ mag, i.e. SDSS J001130.40+005751.80 - $\Delta r = 3.46$ mag, SDSS J023105.597+000843.61 - $\Delta r = 1.02$ mag, SDSS J025515.096+003740.55 - $\Delta r = 1.70$ mag, and SDSS

J235936.817-003112.78 - $\Delta r = 1.20$ mag. In general, the variations in different bands show similar trends, as can be seen from the light curve of SDSS J025515.096+003740.55 for example in Fig. 2. This source has been observed every year from 2000 to 2007. From Fig. 2, the source remained stable in 2000 - 2001, gradually brightening after that. It probably reached its brightest state between the 2004 and 2005 observational runs, after which the source gradually decreased in brightness until reaching its faintest magnitude in 2007. The fluctuations can also be seen in each observational session, for example, there having been about 0.5 mag of amplitude variations in the observational run of 2005.

3.2. Spectral index & brightness relation

The correlation between the spectral index α_{ν} and PSF *r* magnitude was checked for all sources using the Spearman rank correlation analysis method. We found that 15 of 29 FSRQs show a significant correlation at a confidence level of $> 99\%$, of which 14 FSRQs show positive correlations, and only one FSRQ (SDSS J001130.40+005751.7, see next section for details) shows a negative correlation (see Table 1). In contrast, two of the five SSRQs have significant positive correlations at a confidence level of $> 99\%$ (see Table 1).

As an example, the correlation between α_{ν} and *r* magnitude is shown in Fig. 3 for SDSS J025515.096+003740.55. A significant positive correlation can be clearly seen. The Spearman correlation analysis gives a correlation coefficient of $r_s = 0.762$ at a confidence level of $\gg 99.99\%$. This positive correlation means that the source spectra becomes flatter as the source brightens, in other words, the source follows a bluer-when-brighter trend. We noted that the spectral indices are all smaller than 1.0, implying a rising SED in the *ugriz* region, more strictly, in 1755 - 4415 Å wavelength region in the source rest-frame (source redshift $z = 1.0228$). Since the overall variation amplitude $\Delta r = 1.70$ mag is much larger than the typical values of radio-quiet AGNs (e.g. Ai et al. 2010), the variations are most likely to originate from jet nonthermal emissions. Therefore, the bluer-when-brighter trend implies that the synchrotron peak frequency likely increases as the source brightens. Assuming that the source SED in the *ugriz* region closely follows the overall SED of synchrotron emission, $\alpha_{\nu} < 1.0$ means that the synchrotron peak frequency may likely be $\nu_{\text{peak}} > 10^{15.23}$ Hz (i.e. correspond to wavelengths shorter than 1755 Å). This would indicate that this source should be classified as a high-synchrotron-peaked FSRQ which however is not common in FSRQs (Abdo et al. 2010, see also Chen et al. 2009a). Interestingly, we found that 17 of 29 FSRQs have $\alpha_{\nu} < 1.0$ all the time during variability (see Col. 9 of Table 1), thus likely have a high synchrotron peak frequency if their *ugriz* SED closely follows the overall synchrotron SED. Nevertheless, the firm SED classification should be verified by simultaneous multi-band data with a much wider SED coverage.

3.3. SDSS J001130.40+005751.7

As shown in the previous section, SDSS J001130.40+005751.7 is the only FSRQ displaying a negative correlation between the spectral index and *r* magnitude. The negative correlation shows that the source spectrum becomes steeper when the source is brighter, i.e. that there is a redder-when-brighter trend. This source is a known FSRQ, which is included in the Radio Optical X-ray ASDC (ROXA) blazar sample (Turiziani, Cavazzuti & Giommi 2007). It appears as a compact radio source in the NVSS

¹ <http://www.sdss.org/dr7/products/catalogs/flags.html>

and FIRST maps, with a flux density of $f_{\text{FIRST}} = 156.07$ mJy, and $f_{\text{NVSS}} = 167.2$ mJy in FIRST and NVSS, respectively. The spectral index calculated for FIRST 1.4 GHz and PMN 4.85 GHz flux density of $f_{\text{PMN}} = 170$ mJy is $\alpha = -0.07$, while it is $\alpha = 0.13$ when the GB6 4.85 GHz flux density of $f_{\text{GB6}} = 132.76$ mJy is used. It is in the fifth VLBA calibrator survey (VCS5: Kovalev et al. 2007), and is compact in the 8.6 GHz VLBA map, with an integrated flux density of $f_{\text{int}} = 90$ mJy, and a flux density for the unresolved component of $f_{\text{unre}} = 70$ mJy. It is also included in the Combined Radio All-sky Targeted Eight GHz Survey (CRATES: Healey et al. 2007) with $f_{8.4\text{GHz}} = 278.7$ mJy from VLA maps.

The light curves of SDSS J001130.40+005751.7 at u, g, r, i, and z bands are shown in Fig. 4. The variations exhibits similar trends in all bands, over nine years from 1998 to 2007. The overall variation in r band is 3.46 mag, which is shown in Fig. 5. In the observational sessions, the source was brightest at MJD=51081 with $r = 17.49$, while faintest at MJD=54411 with $r = 20.95$. This source seems to vary all the time, with about 1 mag fluctuations in most observational sessions (see Fig. 5).

The negative correlation between the spectral index α_ν and r magnitude is shown in Fig. 6. The Spearman correlation analysis shows a significant negative correlation with a correlation coefficient of $r_s = -0.606$ at confidence level of $> 99.99\%$. This source is included in the first Fermi Large Area Telescope AGN catalogue with a photon index of 2.51 ± 0.15 and classified as a low-synchrotron-peaked FSRQs with $\nu_{\text{peak}} < 10^{14}$ Hz (Abdo et al. 2010). With the source redshift $z = 1.4934$, SDSS *ugriz* wavebands correspond to the wavelength range of 1424 – 3582 Å in the source rest-frame, which is therefore likely at the falling part of synchrotron SED. For a sample of 17 radio-quiet AGNs, Shang et al. (2005) show that the spectral break occurs at around 1100 Å for most objects, which is thought to be closely related to the big blue bump. If this spectral break also exists in SDSS J001130.40+005751.7, we would expect to observe the rising part of accretion disk thermal emission when it dominates over the nonthermal emission. While the spectral index and brightness generally follows an anti-correlation, we note that it is more complex than a simple anti-correlation, as shown in Fig. 6. While the rising optical spectral ($\alpha_\nu < 1.0$) is indeed present at low flux state, the declining spectra ($\alpha_\nu > 1.0$) are also clearly visible at low fluxes. In contrast, the optical spectra decline ($\alpha_\nu > 1.0$) at high flux states, which implies that nonthermal low-peak-frequency synchrotron emission then provides the greatest contribution.

4. Discussions

The bluer-when-brighter trend is commonly observed in blazars, as it has been found by different investigators that the amplitude of the variations is systematically larger at higher frequencies, suggesting that the spectrum becomes steeper when the source brightness decreases, and flatter when it increases (Racine 1970; Gear, Robson & Brown 1986; Ghisellini et al. 1997; Massaro et al. 1998). Investigations of spectral variability have also detected this general trend (D’Amicis et al. 2002; Vagnetti et al. 2003; Fiorucci, Ciprini & Tosti 2004). From our investigations, the variations in the spectral index of 14 of 29 FSRQs indeed follow this trend. This common phenomenon has different possible explanations (Fiorucci et al. 2004). It may indicate the presence of two components that contribute to the overall emission in the optical region, one variable (with a flatter slope α_{var} , where $f_\nu \propto \nu^{-\alpha}$), and the other stable (with $\alpha_{\text{const}} > \alpha_{\text{var}}$). Alternatively,

it may be interpreted using a one-component synchrotron model: the more intense the energy release, the higher the particle’s energy (Fiorucci et al. 2004). Another possible explanation is that the luminosity increase was caused by the injection of fresh electrons, with an energy distribution harder than that of the previous, partially cooled ones (e.g. Kirk, Rieger & Mastichiadis 1998; Mastichiadis & Kirk 2002). Finally, it could be due to Doppler factor variations in a spectrum slightly deviating from a power law, e.g. Doppler factor variations in a ‘convex’ spectrum (Villata et al. 2004).

However, some evidence that the amplitudes of variations are not systematically larger at high frequencies has been found on several occasions (see, for example: Malkan & Moore 1986; Brown et al. 1989; Massaro et al. 1998; Ghosh et al. 2000; Clements et al. 2003; Ramírez et al. 2004). Based on their results, Ghosh et al. (2000) suggested that it may be incorrect to generalize by saying that the amplitude of the variation in blazars is systematically larger at higher frequency. They found that the spectral slope of AO 0235+164 remained almost constant when its brightness increased. In S5 0716+714, while the long-term spectral change is evidently BWB, both BWB chromatism and achromatism were found in both bright and dim source flux states among the microvariability nights (Poon et al. 2009). The authors claimed that the BWB behavior can be explained by the shock-in-jet model, while the achromatic trend may be due to geometric effects. Interestingly, we did not find any significant correlations between spectral index and brightness for 14 FSRQs in our sample.

The redder-when-brighter trend has also been found in several cases (e.g. Gu et al. 2006, Ramírez et al. 2004). The competition between the thermal accretion disk and synchrotron emission was used to explain the RWB trend in FSRQs (Gu et al. 2006). The optical emission of FSRQs is contaminated by thermal emission from the accretion disk. Since FSRQs are usually low-synchrotron-peaked sources with $\nu_{\text{peak}} < 10^{14}$ Hz (Abdo et al. 2010), the big blue bump of accretion disk emission will flatten the spectral slope in the optical region, resulting in a flatter composite spectrum than the non-thermal component. When the object brightens, the non-thermal component has a more dominant contribution to the total flux, and the composite spectrum steepens. The existence of thermal accretion disk emission is supported by the UV excess in 3C 454.3 during lower flux states (Raiteri et al. 2007). The thermal blue bump has also been observed in 3C 345 (Webb et al. 1994). Interestingly, the emergence of accretion disk emission was detected in NLS1s PMN J0948+0022 as its synchrotron emission dropped (Abdo et al. 2009). While the spectral behaviors are not homogenous across our FSRQs sample, it may also be inhomogenous even for a single source. From the four-year five-waveband monitoring, Wu et al. (2010) found both a bluer-when-brighter and redder-when-brighter trend in FSRQ 3C 345 when using a different color index. The RWB trend can be explained by the less variable thermal components. Moreover, the authors argued that the color behaviors of FSRQs are linked not only to their emission process, but also to the redshift and strengths of the less variable thermal components (Wu et al. 2010). Hence, it is most likely that the spectral behaviors of FSRQs depend on the position of the synchrotron peak frequency, the sampled optical wavelength range in the source rest frame (which depends on the redshift), and the positions of thermal blue bump and its strength compared to the jet emission. We note that FSRQs are supposed to display a redder-when-brighter trend, for example, in at least two of three sources, i.e., 3C 454.3 and PKS 0420-014 (Gu et al. 2006), and four of the six sources, PKS 0420-014, 4C 29.45, PKS 1510-

089, and 3C 454.3 (Rani et al. 2010), all of which are known low-synchrotron-peaked FSRQs. In contrast, our results imply that the redder-when-brighter trend may be rarer for FSRQs, at least for our present sample. However, the bluer-when-brighter trend is more common.

Radio-loud quasars, particularly FSRQs, differ from radio-quiet AGNs in terms of their contribution of the nonthermal jet emission in optical continuum emission, in addition to the thermal emission from the accretion disk. In particular, jet emission can be dominant because of the beaming effect when the jet is moving towards us with a small viewing angle. To inspect the continuum emission in our FSRQs, we plot in Fig. 7 the relationship between the continuum luminosity at 3000 Å and broad Mg II line luminosity for 28 FSRQs, both of which are adopted from Shen et al. (2010). For comparison, the ordinary least-square bisector linear fit $\lambda L_{\lambda 3000\text{Å}} = 78.5 L_{\text{Mg II}}^{0.996}$ for a sample of radio-quiet AGNs in Kong et al. (2006) is also plotted with the solid line (see also Chen et al. 2009b). It can be seen that the 3000 Å luminosity of most sources lies above the $\lambda L_{\lambda 3000\text{Å}} - L_{\text{Mg II}}$ relation of radio-quiet AGNs. However, the deviation of $\lambda L_{\lambda 3000\text{Å}}$ is within 0.5 dex. This excess is most likely to be caused by the jet nonthermal emission. The spectra of SDSS J001130.40+005751.7 at MJD=51793 was used to measure the broad emission lines and continuum (Shen et al. 2010), from which the corresponding r magnitude is about 19.6. If the luminosity at 3000 Å of SDSS J001130.40+005751.7 follows the variation amplitude of the r magnitude, we can estimate its highest and lowest values, which are indicated by two rectangles assuming a same Mg II luminosity. Therefore, in the highest flux state, the continuum emission could be dominated completely by the nonthermal emission by more than one order of magnitude (see Fig. 7). However, in the lowest flux state, the thermal emission is likely to be responsible for the continuum emission.

While FSRQs are usually associated with core-dominated radio quasars, SSRQs are generally related to lobe-dominated ones, usually with two large-scale optically thin radio lobes. Usually, the beaming effect is not severe in SSRQs because of the relatively large viewing angle. Therefore, the optical continuum of SSRQs could be dominated by the thermal emission. In Fig. 7, two SSRQs with available Mg II measurements all lie close to but below the solid line for radio quiet AGNs. This likely implies that the thermal emission from accretion disk is indeed dominated in the optical continuum at the epoch of SDSS spectra. Interestingly, two of five SSRQs display a BWB trend (see Table 1). The BWB trend has also been found in radio quiet AGNs, and the variability was found to be anti-correlated with the Eddington ratio (Ai et al. 2010). In radio quiet AGNs, the optical variability could be due to the variation in the accretion process, for example, the variation in the accretion rate (e.g. Li & Cao 2008), since the jet is either weak or absent. These explanations could also be used to explain the variability of SSRQs if the optical emission is indeed mainly from the accretion disk. However, that the variation is caused by jet nonthermal emission cannot be completely excluded in some cases because the variability amplitudes are generally larger than the typical values for radio quiet AGNs (see Table 1). In extreme cases, the overall amplitude is $\Delta r = 0.84$ mag in SDSS J012401.76+003500.9. It may be more likely that both thermal and nonthermal emission contribute to the variability. Further multi-waveband monitoring is needed to help resolve these uncertainties, especially the spectroscopic monitoring.

5. Summary

We have constructed a sample of 32 FSRQs in the SDSS Stripe 82 region. The variability and the relationship between the spectral index and brightness were investigated for 29 FSRQs. We found that all FSRQs show large-amplitude overall variations, e.g. from 0.24 to 3.46 mag at r band. We only found a significant negative correlation between the spectral index and r magnitude (i.e. redder-when-brighter) in one FSRQ, SDSS J001130.40+005751.7. This implies that the RWB trend is rare in our FSRQ sample. This behavior could be explained by the contribution of thermal accretion disk emission in the optical wavebands. In contrast, a bluer-when-brighter trend is more common in FSRQs, and found in 14 of the 29 FSRQs studied here.

Acknowledgements. We thank the anonymous referee for helpful comments and suggestions. MFG thanks R. Antonucci, S. Hönl, J. Wu and Z. Chen for useful discussions. This work is supported by the National Science Foundation of China (grants 10703009, 10821302, 10833002, 10978009, 11033007 and 11073039), and by the 973 Program (No. 2009CB824800). Funding for the SDSS and SDSS-II was provided by the Alfred P. Sloan Foundation, the Participating Institutions, the National Science Foundation, the U.S. Department of Energy, the National Aeronautics and Space Administration, the Japanese Monbukagakusho, the Max Planck Society, and the Higher Education Funding Council for England. The SDSS Web site is <http://www.sdss.org/>.

References

- Abdo, A. A., Ackermann, M., Ajello, M., et al. 2009, *ApJ*, 707, 727
 Abdo, A. A., Ackermann, M., Ajello, M., et al. 2010, *ApJ*, 715, 429
 Abazajian, K. N., Adelman-McCarthy, J. K., Agüeros, M. A., et al. 2009, *ApJS*, 182, 543
 Ai, Y. L., Yuan, W., Zhou, H. Y., et al. 2010, *ApJ*, 716, L31
 Becker, R. H., White, R. L., & Helfand, D. J. 1995, *ApJ*, 450, 559
 Böttcher, M., Basu, S., Joshi, M., et al. 2007, *ApJ*, 670, 968
 Brown, L. M., Robson, E. I., Gear, W. K., & Smith, M. G. 1989, *ApJ*, 340, 150
 Celotti, A., Padovani, P., & Ghisellini, G., 1997, *MNRAS*, 286, 415
 Chen, Z. Y., Gu, M. F., & Cao, X. 2009a, *MNRAS*, 397, 1713
 Chen, Z. Y., Gu, M. F., Fan, Z. H., & Cao, X. W. 2009b, *RAA*, 9, 1192
 Clements, S. D., & Carini, M. T. 2001, *AJ*, 121, 90
 Clements, S. D., Jenks, A., & Torres, Y. 2003, *AJ*, 126, 37
 D’Amicis, R., Nesci, R., Massaro, E., et al. 2002, *PASA*, 19, 111
 Fan, J. H., Xie, G. Z., Pecontal, E., Pecontal, A., & Copin, Y. 1998, *ApJ*, 507, 173
 Fiorucci, M., Ciprini, S., & Tosti, G. 2004, *A&A*, 419, 25
 Francis, P. J., Hewett, P. C., Foltz, C. B., et al. 1991, *ApJ*, 373, 465
 Gear, W. K., Robson, E. I., & Brown, L. M. J. 1986, *Nature*, 324, 546
 Ghisellini, G., Villata, M., Raiteri, C. M., et al. 1997, *A&A*, 327, 61
 Ghisellini, G., Tavecchio, F., Foschini, L., et al. 2010, *MNRAS*, 402, 497
 Ghosh, K. K., Ramsey, B. D., Sadun, A. C., & Soundararajaperumal, S. 2000, *ApJS*, 127, 11
 Gregory, P. C., Scott, W. K., Douglas, K., & Condon, J. J. 1996, *ApJS*, 103, 427
 Griffith, M. R., & Wright, A. E. 1993, *AJ*, 105, 1666
 Griffith, M. R., Wright, A. E., Burke, B. F., & Ekers, R. D. 1995, *ApJS*, 97, 347
 Gu, M. F., Lee, C.-U., Pak, S., Yim, H. S., & Fletcher, A. B. 2006, *A&A*, 450, 39
 Healey, S. E., Romani, R. W., Taylor, G. B., et al. 2007, *ApJS*, 171, 61
 Hu, S. M., Zhao, G., Guo, H. Y., Zhang, X., & Zheng, Y. G. 2006, *MNRAS*, 371, 1243
 Ivezić, Ž., Menou, K., Knapp, G. R., et al. 2002, *AJ*, 124, 2364
 Kimball, A. E., & Ivezić, Ž. 2008, *AJ*, 136, 684
 Kirk, J. G., Rieger, F. M., & Mastichiadis, A. 1998, *A&A*, 333, 452
 Kong, M. Z., Wu, X. B., Wang, R., & Han, J. L. 2006, *Chinese J. Astron. Astrophys.*, 6, 396
 Kovalev, Y. Y., Petrov, L., Fomalont, E. B., & Gordon, D. 2007, *AJ*, 133, 1236
 Li, S. L., & Cao, X. W. 2008, *MNRAS*, 387, L41
 Lu, Y., Wang, T., Zhou, H., & Wu, J. 2007, *AJ*, 133, 1615
 Lupton, R. H., Ivezić, Ž., Gunn, J. E., et al. 2002, *Proc. SPIE*, 4836, 350
 Malkan, M., & Moore, R. 1986, *ApJ*, 300, 216
 Massaro, E., Nesci, R., Maesano, M., Montagni, F., & D’Alessio, F. 1998, *MNRAS*, 299, 47
 Mastichiadis, A., & Kirk, J. G. 2002, *PASA*, 19, 138
 Miller, H. R. 1981, *ApJ*, 244, 426

- Neter, H. 1990 in *Active Galactic Nuclei*, ed. R. D. Blandford et al. (Berlin: Springer), 57
- Osterman Meyer, A., Miller, H. R., Marshall, K., et al. 2008, *AJ*, 136, 1398
- Osterman Meyer, A., Miller, H. R., Marshall, K., et al. 2009, *AJ*, 138, 1902
- Poon, H., Fan, J. H., & Fu, J. N. 2009, *ApJS*, 185, 511
- Racine, R. 1970, *ApJ*, 159, L99
- Raiteri, C. M., Villata, M., Aller, H. D., et al. 2001, *A&A*, 377, 396
- Raiteri, C. M., Villata, M., Larionov, V. M., et al. 2007, *A&A*, 473, 819
- Ramírez, A., de Diego, J. A., Dultzin-Hacyan, D., & González-Pérez, J. N. 2004, *A&A*, 421, 83
- Rani, B., Gupta, A. C., Strigachev, A., et al. 2010, *MNRAS*, 404, 1992
- Schneider, D. P., Richards, G. T., Hall, P. B., et al. 2010, *AJ*, 139, 2360
- Shakura, N. I., & Sunyaev, R. A. 1973, *A&A*, 24, 337
- Shang, Z. H., Brotherton, M. S., Green, R. F., et al. 2005, *ApJ*, 619, 41
- Shen, Y., Hall, P. B., Richards, G. T., et al. 2010, arXiv: 1006.5178
- Stalin, C. S., Gopal-Krishna, Sagar, R., et al. 2006, *MNRAS*, 366, 1337
- Turiziani, S., Cavazzuti, E., & Giommi, P. 2007, *A&A*, 472, 699
- Vagnetti, F., Trevese, D., & Nesci, R. 2003, *ApJ*, 590, 123
- Vestergaard, M., & Peterson, B. M. 2006, *ApJ*, 641, 689
- Villata, M., Raiteri, C. M., Kurtanidze, O. M., et al. 2002, *A&A*, 390, 407
- Villata, M., Raiteri, C. M., Kurtanidze, O. M., et al. 2004, *A&A*, 421, 103
- Webb, J. R., Shrader, C. R., Balonek, T. J., et al. 1994, *ApJ*, 422, 570
- Wu, J. H., Peng, B., Zhou, X., et al. 2005, *AJ*, 129, 1818
- Wu, J. H., Zhou, X., Ma, J., et al. 2007, *AJ*, 133, 1599
- Wu, J. H., et al., 2010, in preparation

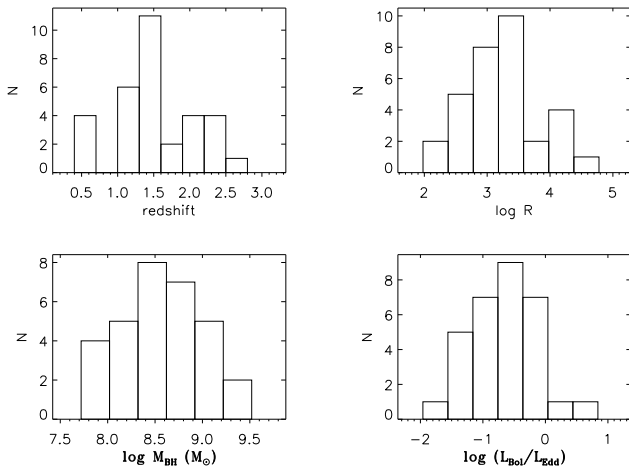


Fig. 1. The histogram of sample parameters: redshift (upper left), radio loudness (upper right), black hole mass (lower left), and the Eddington ratio (lower right). SDSS J222646.53+005211.3 is not included in the histogram of black hole mass and Eddington ratio because of the lack of broad emission-line measurements.

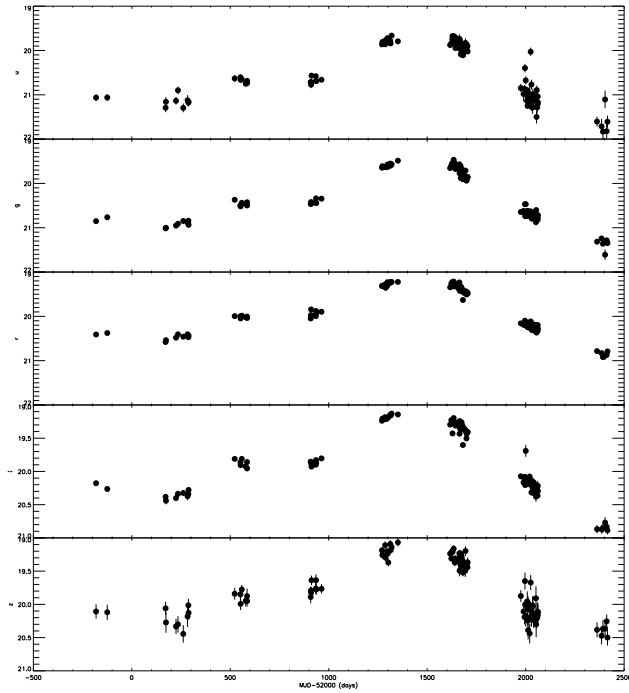


Fig. 2. The *ugriz* band light curve of SDSS J025515.09+003740.5 (from top to bottom).

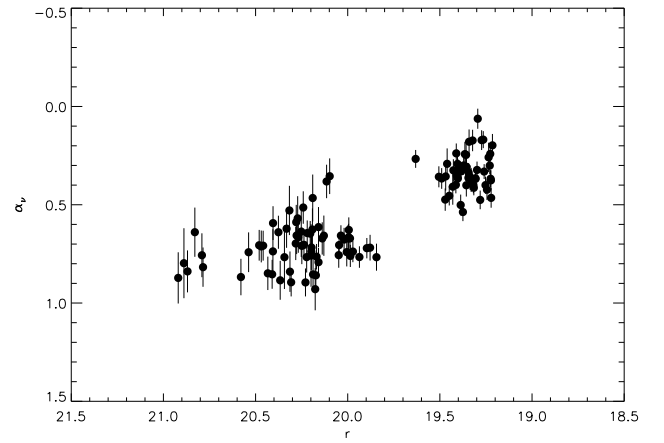


Fig. 3. The relationship between the spectral index and the PSF magnitude at *r* band for SDSS J025515.09+003740.5. A significant positive correlation is present, which implies a bluer-when-brighter trend.

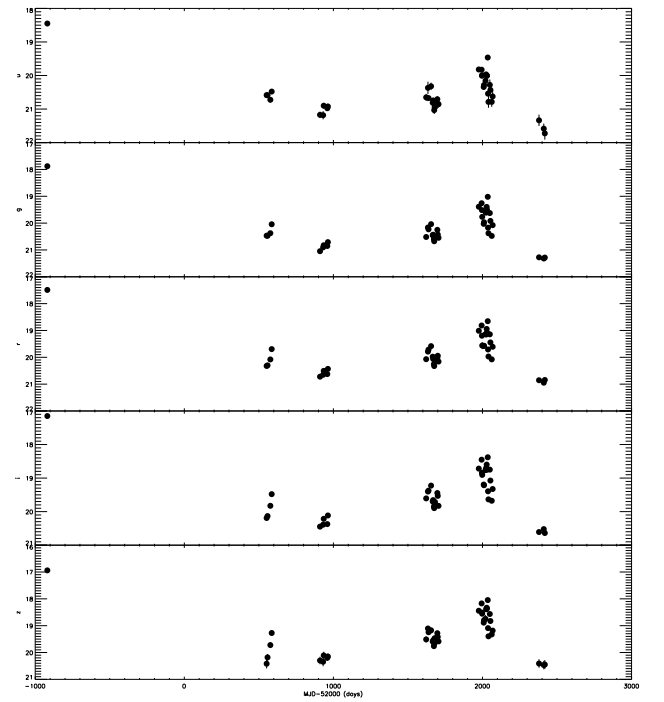


Fig. 4. The *ugriz* band light curve of SDSS J001130.40+005751.7 (from top to bottom).

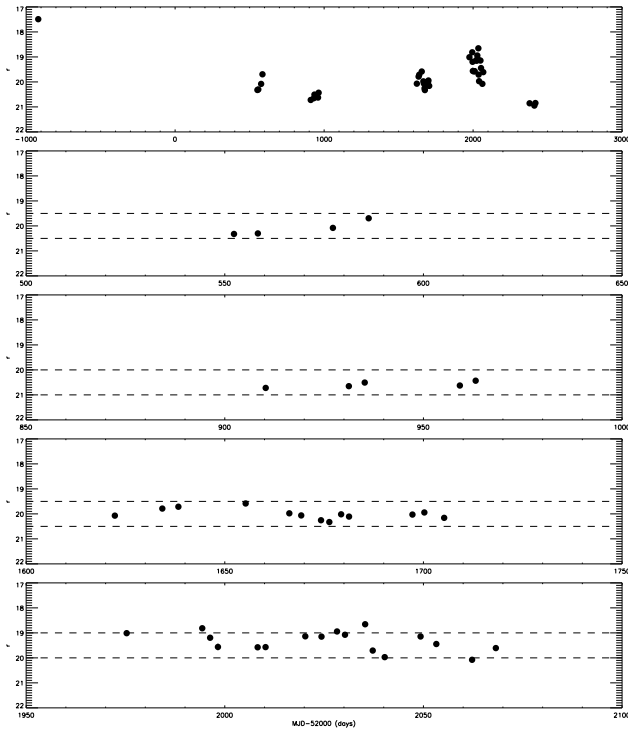


Fig. 5. The r band light curve of SDSS J001130.40+005751.7. The light curves of the second to fifth observational sessions are zoomed in the second to fifth panels from up to bottom. The dashed lines represent 1 mag variations.

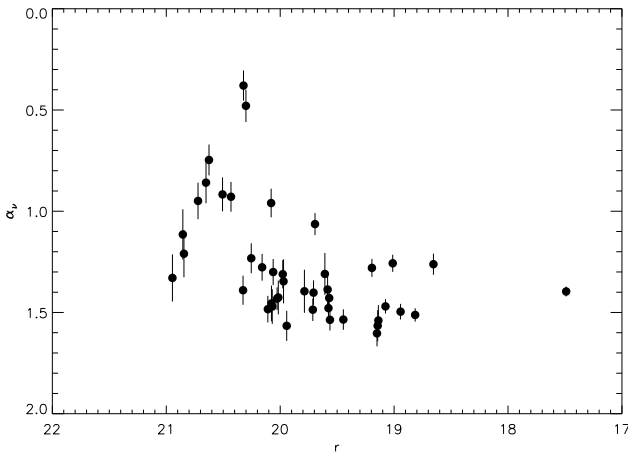


Fig. 6. The relationship between the spectral index and the PSF magnitude at r band for SDSS J001130.40+005751.7. A significant anti-correlation is present, which implies a redder-when-brighter trend.

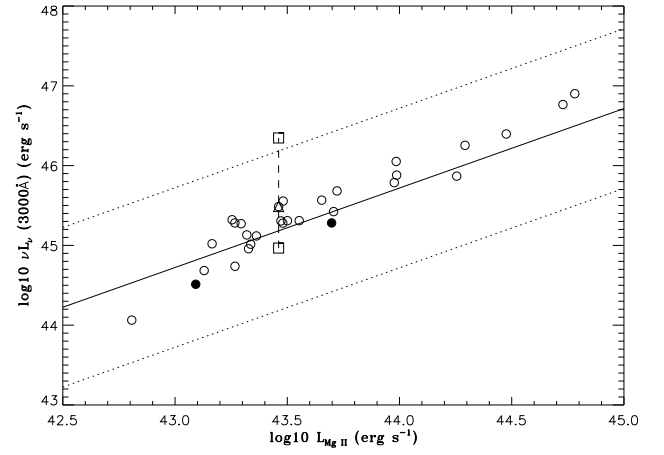


Fig. 7. The plot of broad Mg II line luminosity and continuum luminosity at 3000 \AA . The solid line is the OLS bisector linear fit to radio-quiet AGNs in Kong et al. (2006), $\lambda L_{\lambda 3000 \text{ \AA}} = 78.5 L_{\text{Mg II}}^{0.996}$. The open circles are FSRQs, solid circles are SSRQs, and open triangle is SDSS J001130.40+005751.7. The vertical dashed line represents the luminosity range at 3000 \AA assuming its variation is identical to that in the r band, which is connected by two rectangles. The dotted lines show the one order of magnitude deviation of continuum luminosity at 3000 \AA from the solid line.

Table 1. Source list: Col. 1 - SDSS source name; Col. 2 - redshift; Col. 3 - radio loudness; Col. 4 - the spectral index between 1.4 and 4.85 GHz, of which PMN flux density is used for those labeled with ^a, otherwise GB6 one is used; Col. 5 - black hole mass in unit of solar mass; Col. 6 - disc bolometric luminosity in unit of erg s⁻¹; Col. 7 - the Eddington ratio $l = L_{\text{BOL}}/L_{\text{EDD}}$; Col. 8 - overall variation in r band; Col. 9 - the range of variation in the spectral index α_v ; Cols. (10-11) - the Spearman correlation coefficient and probability level, respectively.

SDSS source	z	$\log_{10}(R)$	α_r	$\log_{10}(M_{\text{BH}})$	$\log_{10}(L_{\text{BOL}})$	$\log_{10}(l)$	Δr	$\Delta \alpha_v$	r_s	prob.
(1)	(2)	(3)	(4)	(5)	(6)	(7)	(8)	(9)	(10)	(11)
J001130.40+005751.7	1.4934	3.42	0.13	8.59	45.67	-1.02	3.45	0.38,1.60	-0.606	0.16e-04
J001611.08-001512.4	1.5759	4.26	0.32 ^a	8.40	45.91	-0.60	0.55	0.86,1.74	0.250	0.11
J002509.66-004031.0	2.2086	3.21	0.25 ^a	8.54	46.41	-0.24	0.37	0.28,0.71	0.310	0.16e-01
J003443.92-005413.0	0.6561	3.03	-0.63 ^a	8.84	45.41	-1.54	0.50	-0.19,0.52	-0.167	0.15
J003512.90+010430.6	2.2603	3.45	0.49	8.77	45.85	-1.04	0.34	0.71,1.35	0.209	0.29
J004332.71+002459.8	1.1277	3.21	0.09	8.02	45.47	-0.67	0.47	-0.28,1.24	0.452	0.20e-07
J004819.12+001457.1	1.5450	3.45	-0.06 ^a	8.36	45.93	-0.55	0.52	0.02,0.90	0.769	0.29e-13
J005205.56+003538.1	0.3993	1.97	0.01	8.51	45.97	-0.65	0.44	0.83,1.49	-0.100	0.47
J005716.99-002433.2	2.7316	2.93	-0.42 ^a	9.11	46.68	-0.55	0.49	0.17,0.77	-0.107	0.46
J011129.94+003431.3	1.3203	2.47	-0.59	8.00	45.94	-0.18	0.54	0.11,0.97	-0.007	0.95
J012401.76+003500.9	1.8516	3.85	0.86	9.36	46.11	-1.36	0.84	-0.52,0.61	0.687	0.68e-06
J012517.14-001828.9	2.2780	3.44	0.59 ^a	8.50	47.13	0.52	0.29	0.22,0.87	-0.202	0.11
J012528.84-000555.9	1.0759	3.16	0.12 ^a	9.13	46.69	-0.55	0.50	-0.59,0.25	0.012	0.91
J012753.70+002516.4	2.4566	3.46	0.42 ^a	7.82	46.51	0.57	0.62	-0.34,0.49	0.216	0.42e-01
J015243.14+002039.6	0.5776	3.95	0.15	8.16	45.02	-1.26
J015454.36-000723.1	1.8287	3.52	0.32 ^a	8.46	46.47	-0.10	0.73	0.16,0.91	0.382	0.90e-03
J015832.51-004238.2	2.6071	3.58	0.87 ^a	8.29	46.90	0.50	0.47	0.44,1.19	-0.207	0.28
J021728.62-005227.2	2.4621	3.29	0.75 ^a	8.84	46.40	-0.55	0.35	0.45,1.28	0.488	0.77e-05
J022508.07+001707.2	0.5270	3.81	0.86	8.88	45.19	-1.80	0.53	0.25,0.68	0.470	0.27e-01
J023105.59+000843.5	1.3354	3.03	0.10 ^a	8.63	45.77	-0.98	1.02	0.09,0.76	0.663	0.10e-07
J025515.09+003740.5	1.0228	2.86	-0.78	8.73	45.55	-1.29	1.70	0.06,0.93	0.761	0.46e-22
J213638.58+004154.2	1.9397	3.69	-0.87	9.11	47.29	0.07	0.28	0.12,0.52	0.581	0.10e-06
J215349.75+003119.5	1.8144	3.56	0.37	8.32	46.07	-0.36
J221001.81-001309.7	1.0941	3.54	0.31 ^a	7.84	45.54	-0.41	0.47	0.19,1.07	0.476	0.33e-02
J221806.67+005223.5	1.2734	2.04	-0.23	8.69	46.51	-0.30	0.26	-0.07,0.33	0.656	0.87e-09
J222235.84+001536.3	1.3617	3.28	0.24 ^a	8.83	45.53	-1.41	0.65	0.20,1.21	0.778	0.33e-08
J222646.53+005211.3	2.26	4.48	0.15
J222713.23-005041.4	1.5063	2.62	-1.12 ^a	8.75	45.78	-1.08	0.87	0.60,1.89	0.766	0.15e-13
J222744.58+003450.8	1.5488	2.67	-0.57	8.11	45.64	-0.59	0.65	-0.01,0.91	0.581	0.46e-06
J224146.37+001608.0	1.4985	3.08	-0.06 ^a	7.72	45.51	-0.33	0.40	-0.07,0.78	0.761	0.77e-08
J231222.36-010924.8	1.4309	4.24	0.37 ^a	8.44	45.58	-0.98	0.28	1.44,2.47	-0.068	0.73
J232037.99+003139.7	1.8993	2.99	-0.18	9.07	46.55	-0.64	0.47	0.23,0.95	0.267	0.38e-01
J232659.08-002352.4	2.1598	3.98	0.24 ^a	8.36	45.52	-0.96	0.24	0.98,1.29	0.142	0.78
J232734.73+002234.0	1.4939	2.56	0.06	9.27	46.20	-1.19	0.48	0.23,0.86	0.501	0.71e-05
J234023.66-005326.9	2.0853	2.38	-0.30 ^a	9.10	46.96	-0.25	0.28	0.54,1.34	0.536	0.70e-05
J235409.17-001947.9	0.4615	3.13	-0.03 ^a	9.28	45.44	-1.96	0.73	0.38,1.00	0.321	0.10e-01
J235936.81-003112.7	1.0956	4.01	-0.51 ^a	8.12	45.34	-0.89	1.19	0.64,1.05	0.571	0.13